Lifetime study of particle-hole excitations in the semimagic nucleus ^{94}Ru

A. Jungclaus, D. Kast, K. P. Lieb, C. Teich, and M. Weiszflog*
II. Physikalisches Institut, Universität Göttingen, Bunsenstrasse 7-9, D-37073 Göttingen, Germany

T. Härtlein, C. Ender, F. Köck, and D. Schwalm
Max-Planck Institut für Kernphysik, D-69029 Heidelberg, Germany

I. P. Johnstone
Department of Physics, Queen's University, Kingston, Ontario, Canada K7L 3N6

J. Reif and R. Schwengner
Institut für Kern- und Hadronenphysik, FZ Rossendorf, D-01314 Dresden, Germany

R. Peusquens, A. Dewald, J. Eberth, and H. G. Thomas
Universität zu Köln, Zülpicher Strasse 77, D-50937 Köln, Germany

M. Górska and H. Grawe
Gesellschaft für Schwerionenforschung, D-64291 Darmstadt, Germany
(Received 12 February 1999; published 16 June 1999)

The recoil-distance Doppler-shift technique was employed to determine lifetimes of high-spin states in the semimagic nucleus ^{94}Ru. The nuclei were populated using the reaction ^{58}Ni(^{40}Ca,$4p$) at a beam energy of 145 MeV, and the γ radiation from their decay was detected in six EUROBALL cluster detectors. A total of 23 reduced transition probabilities and limits for fifteen further transitions were extracted and compared to large-scale shell model calculations, considering different configuration spaces and residual interactions. The information deduced on transition strengths turned out to be essential for the correct assignment of the calculated to the experimental excited states. The results indicate that the 13_2^- (6919 keV), 14_1^- (7970 keV), and the 15_1^- (8133 keV) levels have pure proton $\pi(f_{5/2})^{-1}\ \pi(g_{9/2})^5$ configurations, whereas all other excited states above 6.3 MeV are built from a neutron $g_{9/2}\rightarrow d_{5/2}$ excitation across the $N=50$ shell closure, coupled to up to six valence protons. Strong $M1$ transitions were found in a stretched dipole cascade within the sequence of neutron core-excited states at positive parity, while the strengths of the transitions between core-excited and pure proton states were proven to be small, similar as in ^{95}Rh. [S0556-2813(99)03007-1]

PACS number(s): 21.10.Ky, 21.60.Cs, 24.70.+s, 27.50.+e

I. INTRODUCTION

Following our investigation of ^{95}Rh [1], with the present paper we continue the studies of the electromagnetic decay properties of neutron core-excited states in $N=50$ nuclei with the presentation of experimental lifetimes in the neighboring nucleus ^{94}Ru. After a first in-beam study of ^{94}Ru by Nolte *et al.* [2], the level scheme of this nucleus has been extended up to spins 21^+ and 25^- by Roth *et al.* [3], using the NORDBALL spectrometer in combination with both neutron and charged particle detectors. Figure 1 shows that part of the excitation scheme obtained in Ref. [3] which is relevant for the present work. The maximum spins that can be built by the six protons within the $(g_{9/2},p_{1/2})$ space are 12^+, 13^- and only a few units larger $(15^+,15^-)$ when additionally including the $p_{3/2}$ and $f_{5/2}$ orbits. For that reason, it is generally assumed that the higher-spin states require the breaking of the $N=50$ closed neutron core, i.e., the excitation of a neutron from the $g_{9/2}$ into the $d_{5/2}$ orbit. Following the experimental work by Roth *et al.* [3], both Ghugre and Datta [4] and Johnstone and Skouras [5] performed shell model calculations allowing for such a neutron excitation across the shell gap. However, due to the high level density observed experimentally, especially above 7 MeV at negative parity, a thorough comparison between calculation and experiment solely based on the excitation energies turned out to be very difficult.

Since only little lifetime information was available for ^{94}Ru [2], we performed a coincidence lifetime measurement employing the RDDS technique and six highly efficient EUROBALL cluster detectors to determine accurate absolute transition strengths, especially at very high spin. On the basis of this new experimental information, it was then possible to evaluate the shell model structure of ^{94}Ru and to differentiate between the various structures in the spin range $12-18\hbar$, where the level density is very high.

II. EXPERIMENT

The reaction ^{58}Ni(^{40}Ca,$4p$) was used to populate excited states in ^{94}Ru using a 3 particle nA 145 MeV $^{40}Ca^{10^+}$ beam provided by the Heidelberg MP-tandem accelerator. A

*Present address: The Svedberg Laboratory, Uppsala University, Sweden.

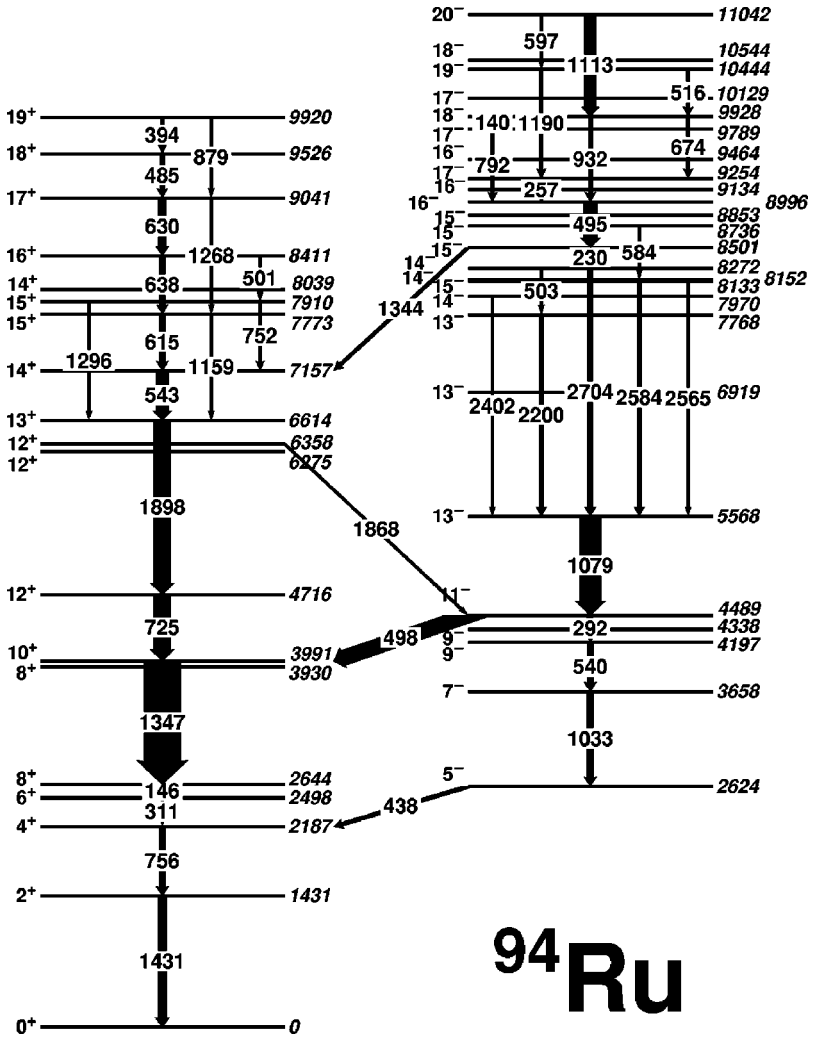

FIG. 1. Relevant part of the level scheme of ^{94}Ru deduced in Ref. [3]. Only the strongest transitions are included.

1.0 mg/cm^2 stretched ^{58}Ni target foil (enrichment 99.9%) and a 16.6 mg/cm^2 stretched Ta stopper foil were mounted in the Cologne plunger device [6] and data were taken at fifteen different flight distances in the range from 15 μm to 10 mm. The recoil velocity was deduced from the energy shift between stopped and Doppler-shifted components of intense γ transitions in ^{94}Ru to be $v/c=2.64(8)\%$ [$v=7.93(24)$ μm/ps]. At a beam energy of 145 MeV, ^{94}Ru is produced in the strongest reaction channel, collecting about half of the total fusion cross section. The lifetime results for the $3p$ channel ^{95}Rh (19%) and the $\alpha 2p$ channel ^{92}Ru (10%) have recently been published elsewhere [1,7]. To complement the RDDS measurement with information concerning shorter lifetimes, data were also taken using a 300 μg/cm^2 gold-backed ^{58}Ni target in order to search for Doppler-broadened line shapes. However, no such DSA line shapes were observed in ^{94}Ru up to the highest observed levels with spin 19^+ and 20^-, respectively.

The γ rays were detected in six EUROBALL cluster detectors [8] which were arranged in two groups of three clusters each, centered at 41° and 139° with respect to the beam. With a target-cluster distance of 22 cm, this 2×3-cluster setup [9] has a total photopeak efficiency of 5.9% at 1.3 MeV γ-ray energy. Besides the high efficiency, this setup is especially well suited for Doppler-shift experiments because all Ge crystals are positioned at angles where the shifted components are well separated from the unshifted ones, even at rather low γ energies.

III. DDCM ANALYSIS AND RESULTS

Details about the data treatment were already given in our previous publication discussing the results for ^{95}Rh deduced from the same data set [1]. Here we will only give a brief description of the most important steps. To fully exploit the efficiency of the setup for high energy γ rays, the cluster detectors were operated in add-back mode [8]. Whenever two neighboring Ge crystals in a cluster registered γ rays within a time window of about 100 ns, the two signals were assumed to originate from the same Compton-scattered incident γ ray and were summed up (''added back'') to give a full energy event. This procedure leads to an energy dependent increase in efficiency, e.g., a factor of 2 in counting rate for the 1898 keV $13^+\rightarrow12^+$ transition in ^{94}Ru (compare Ref. [1]). For each of the fifteen flight distances, two symmetric matrices (41° versus 41°, 139° versus 139°) and one

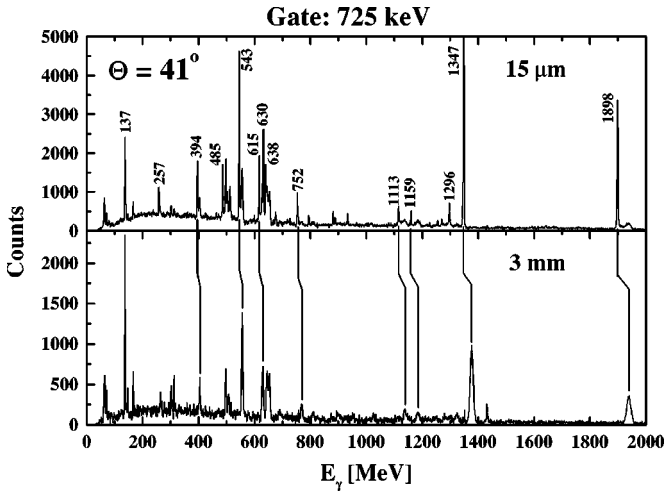

FIG. 2. Coincidence spectra with gates set on both the shifted and the unshifted part of the 725 keV, $12^+ \rightarrow 10^+$ transition in ^{94}Ru for the three forward clusters at flight distances of 15 μm (upper part) and 3 mm (lower part).

asymmetric matrix (41° versus 139°) were sorted leading to a set of four independent coincidence spectra for each pair of coincident γ rays corresponding to the four possible combinations of detecting the ''gate'' and the ''look'' transition at forward or backward angle. As an example, Fig. 2 shows the spectra obtained in the three forward clusters in coincidence with both the Doppler-shifted and unshifted parts of the 725 keV $12^+ \rightarrow 10^+$ γ ray at flight distances of 15 μm and 3 mm. All γ rays in coincidence with the 725 keV transition decay during the flight for the distance of 3 mm and therefore appear as completely shifted lines in that spectrum. Note that the $8^+ \rightarrow 6^+ \rightarrow 4^+ \rightarrow 2^+ \rightarrow 0^+$ cascade is not observed in this spectrum. Due to the long lifetime of the isomeric 8^+ state ($T_{1/2}=71$ μs [10]) compared to the coincidence time window, no coincidences between the γ rays above and below the 8^+ isomer occur. As an example at negative parity, the spectra taken at 15 μm and 10 mm in coincidence with the 1079 keV $13^- \rightarrow 11^-$ transition are given in Fig. 3. Whereas the 292, 540, and 1033 keV transitions below the 11^- level show both unshifted and shifted parts at 10 mm flight distance, the 438, 756, and 1431 keV γ rays were only emitted after the nuclei had come to rest in the stopper even at this long distance due to the 1.1 ns and 0.73 ns lifetimes of the 4489 keV 11^- and 2624 keV 5^- states, respectively (compare Table I). The intensities in the coincidence spectra taken at the fifteen target-to-stopper distances were normalized to the sum of the unshifted and shifted components of strong transitions in ^{95}Rh in coincidence spectra with gates set on γ rays depopulating the isomeric $17/2^-$ state [$\tau = 27(1)$ ns [11]] as described in Ref. [1].

Since the counting statistics obtained for the strong reaction channels in the present experiment was very high, it was possible to apply the differential decay curve method (DDCM) [12] in the lifetime analysis, thus avoiding systematical uncertainties concerning cascade and side feedings. The lifetime of a state can be deduced for each target-to-stopper distance x independently from the coincidence intensities of γ rays feeding and depopulating the level of interest. If $\gamma_{\rm in}$ denotes a direct feeding transition and $\gamma_{\rm out}$ a γ-ray depopulating the state, the lifetime can be calculated from the equation

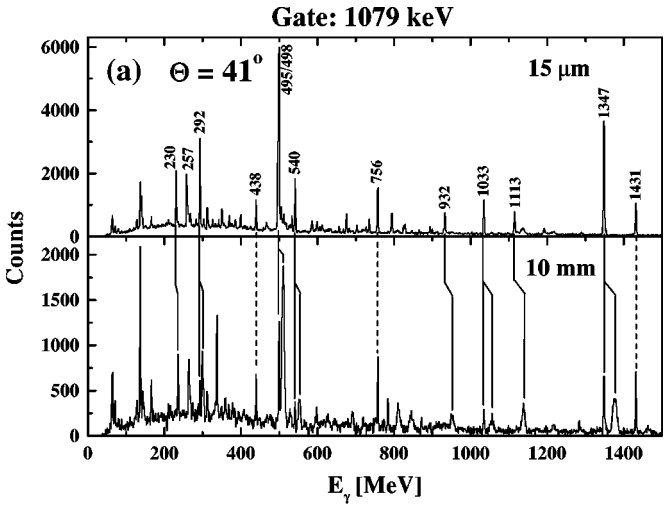

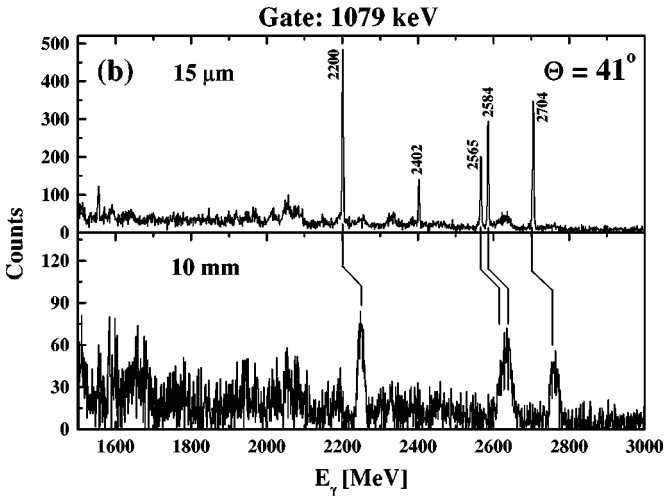

FIG. 3. Coincidence spectra with gates set on both the shifted and the unshifted part of the 1079 keV, $13^- \rightarrow 11^-$ transition in ^{94}Ru for the three forward clusters at flight distances of 15 μm (upper part) and 10 mm (lower part); (a) low-energy part, (b) high-energy part.

$$\tau(x)=\frac{1}{v}\quad\frac{I(\gamma_{\rm out}^{\rm unshifted},\gamma_{\rm in}^{\rm shifted};x)}{dI(\gamma_{\rm out}^{\rm shifted},\gamma_{\rm in}^{\rm shifted};x)/dx}, \tag{1}$$

where $I(\gamma_{\rm out}^{\rm unshifted},\gamma_{\rm in}^{\rm shifted};x)$ is the intensity of the unshifted (stop) component of transition $\gamma_{\rm out}$ in the coincidence spectrum with the gate set on the Doppler-shifted (flight) component of transition $\gamma_{\rm in}$. The denominator is derived from a fit of a product of exponential decay functions to the discrete values of $I(\gamma_{\rm out}^{\rm shifted},\gamma_{\rm in}^{\rm shifted};x)$ for the different distances x. The lifetime is finally calculated by averaging the τ values obtained for the distances within the region of highest sensitivity. The DDCM analysis is illustrated in Fig. 4, where three examples are given. For each level of interest three curves are shown: the intensity of the unshifted part of the

TABLE I. Lifetimes of excited states in ^{94}Ru as obtained in this work. The energy and spin/parity of the state are given in the first and second column, respectively. The third column indicates the energy of the depopulating γ ray used in the lifetime determination. τ (column 4) is the state lifetime determined via the DDCM method. In the last column, the results from Ref. [2] are quoted.

E_x (keV)	I^π	E_γ (keV)	τ (ps)	$\tau_{\rm lit}$ (ps)
		Positive parity		
3991	10^+	1347	<5	
4716	12^+	725	34.3(16)	50(4)
6614	13^+	1898	1.26(17)	
7157	14^+	543	0.48(6)	
7773	15^+	1159	<0.4	
8411	16^+	638	<1	
9041	17^+	630	<2	
9526	18^+	485	0.52(3)	
9920	19^+	394	<4.9	
		Negative parity		
2624	5^-	438	731(67)	$765(^{721}_{289})$
4489	11^-	292	1097(50)	1125(173)
5568	13^-	1079	2.90(32)	
8272	14^-_3	2704	0.42(4)	
8501	15^-_2	230	1.84(12)	
8996	16^-	495	<1	
9928	18^-	932	5.04(34)	
11042	20^-	1113	<2.6	

depopulating transition in coincidence with the shifted component of a direct feeder is displayed in the upper part [numerator of Eq. (1)]. The slope of the intensity of the shifted part of the depopulating γ ray with the same coincidence requirement is given in the middle row [denominator of Eq. (1)]. Finally, the individual τ values as calculated using Eq. (1) are shown in the lower part of the figure. The region of highest sensitivity, i.e., largest values for both the numerator and the denominator of Eq. (1), is marked by dashed vertical lines.

This DDCM method is a very elegant way of deducing lifetimes from coincidence data. However, it is very important to very carefully check the coincidence spectra with the gates set on the Doppler-shifted parts of the feeding transition for contaminations. In view of the quite large energy widths of these gates and the high line density observed in the reaction employed, such contaminations often occur and lead to the rejection of the respective spectrum. For example, in the gate set on the shifted component of the 495 keV $16^-_1 \rightarrow 15^-_2$ transition in forward direction ($\Theta = 41°$), the spectrum also contains contributions from coincidences with the 498 keV $11^- \rightarrow 10^+$ and the 503 keV $14^-_3 \rightarrow 13^-_3$ γ rays. Therefore, only those spectra with the gate in backward direction were used for the determination of the lifetime of the 15^-_2 state. The situation is particularly complicated for the $17^+ \rightarrow 16^+ \rightarrow 15^+_1 \rightarrow 14^+_1$ cascade due to the small energy spacing between the transitions involved (630, 638, and 615 keV). In Fig. 5, this energy region is shown in the coincidence spectrum with a gate on the 725 keV $12^+ \rightarrow 10^+$ transition for the two angles of observation and two flight distances, namely, 15 μm and 3 mm. It is obvious from this figure that there is no possibility to observe both the unshifted and the shifted part of the 630 keV γ ray at the same time without contaminations. As a consequence, the lifetime of the 17^+ state could only be estimated from the spectra to be shorter than 2 ps. The lifetime of the 16^+ level was estimated to be <1 ps from the fact that no unshifted peak of the 638 keV γ ray was observed in coincidence with the shifted part of the 630 keV line at any of the flight distances. For the determination of the 15^+ lifetime the gate was set on the shifted part of the 638 keV feeding transition. At backward angles, this gate also contains components of the 630 keV $17^+ \rightarrow 16^+$ γ ray (compare Fig. 5) and cannot be used. At forward direction, the gate is contaminated by the 650 keV $13^+ \rightarrow 12^+$ transition in ^{94}Rh. Since this transition is in coincidence with the 617 keV $12^+ \rightarrow 10^+$ γ ray in ^{94}Rh, the 615 keV $15^+ \rightarrow 14^+$ γ ray in ^{94}Ru cannot be used for the determination of the 15^+ lifetime. Only the much weaker, depopulating 1159 keV transition could be considered, leading to the limit $\tau(15^+) < 0.4$ ps. In the case of the 14^+ level, only the backward detectors were used for gating the Doppler-shifted 615 keV $15^+ \rightarrow 14^+$ line since, at $\Theta = 41°$, this gate also contains the unshifted part of the 630 keV $17^+ \rightarrow 16^+$ line (see Fig. 5). The lifetime of the 13^- state was determined from gates set both on the 2704 keV and the 2200 keV feeding transitions, leading to an average value of $\tau(13^-) = 2.90(32)$ ps.

All the lifetime results obtained in this work are summarized in Table I and compared to the three values measured by Nolte *et al.* [2]. In Table II, the reduced electromagnetic transition probabilities derived from the experimental results are presented, making use of the branching ratios published in Ref. [3]. For the $\Delta I = 0$ and $\Delta I = 1$ transitions, the unknown mixing ratios were set to zero. In view of the mainly strong $M1$ and weak $E2$ transitions in this nucleus, this assumption seems well justified.

IV. DISCUSSION

To describe the level scheme of ^{94}Ru up to spins as high as 19^+ and 20^-, neutron excitations across the $N = 50$ shell gap have to be considered. On the proton side, excitations from the $f_{5/2}$ and $p_{3/2}$ orbits into the $g_{9/2}$ shell might also be of importance. To facilitate the discussion, we will classify the possible configurations in the following way: states built from protons within the $(p_{1/2}, g_{9/2})$ space with an inert neutron core will be called core states. States containing a neutron $d_{5/2}$ particle-hole excitation will be referred to as νph and those which are dominated by proton $f_{5/2}, p_{3/2} \rightarrow g_{9/2}$ excitations as πph states. Finally, levels with significant contributions from both neutron and proton excitations will be called $\pi\nu ph$. In the following we will discuss three different shell model calculations. All three approaches have in common that they indicate that all the states observed up to the yrast 12^+ (4716 keV) and 13^- (5568 keV) levels are core states having nearly pure $\pi(g_{9/2})^4$ and $\pi(p_{1/2})^{-1}\pi(g_{9/2})^5$ configurations, respectively. They also reproduce the high

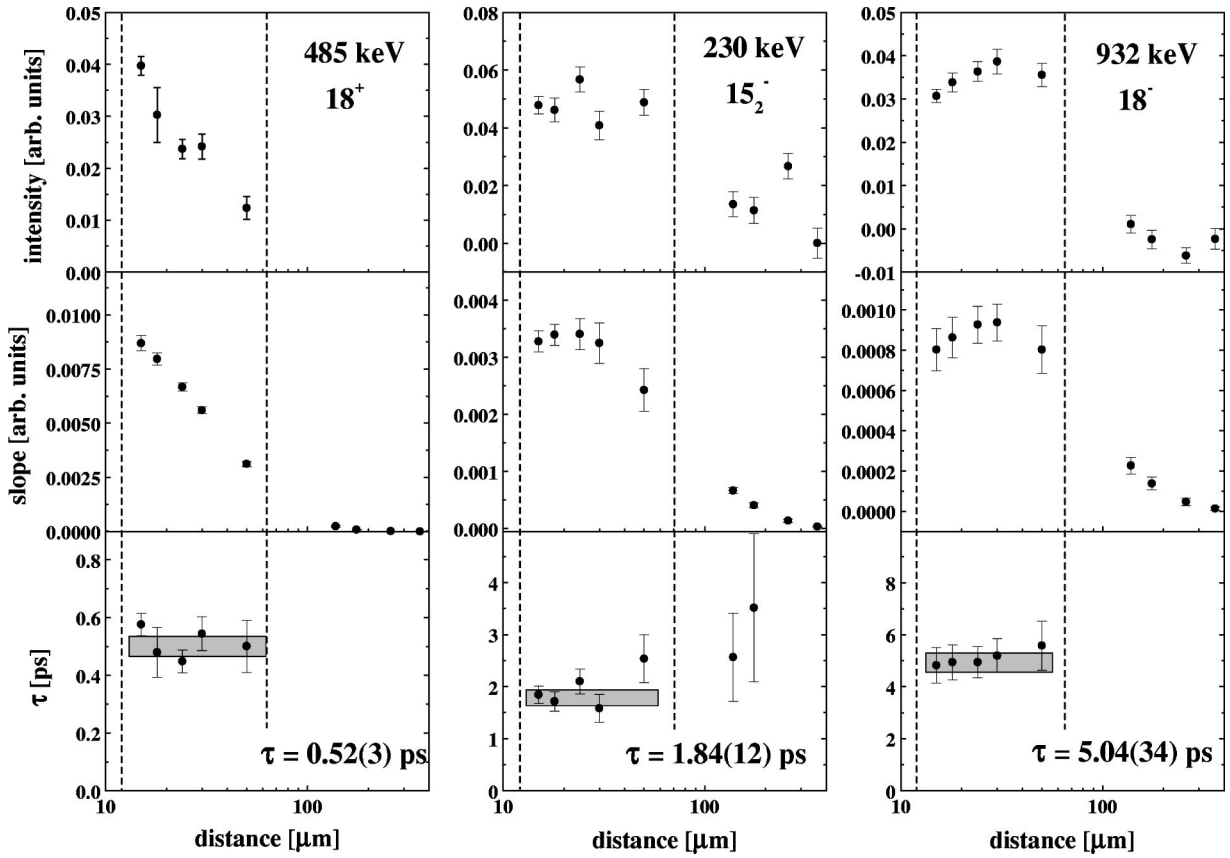

FIG. 4. DDCM analysis of the data for the 18^+, 15_2^-, and 18^- levels referring to the 485, 230, and 932 keV transitions. The lifetimes obtained are shown in the lower parts where the τ curves are displayed and the average values with their errors are indicated by grey boxes. The region of highest sensitivity is marked by vertical dashed lines. For more details see text.

level density observed experimentally at negative parity above 7.5 MeV. However, they do not agree concerning the predicted structures of some states at higher excitation energies.

A. Shell model calculation by Ghugre and Datta

Ghugre and Datta [4] presented calculations for the $N=50$ isotones ^{92}Mo, ^{93}Tc, ^{94}Ru, and ^{95}Rh, using as configuration space the orbits $f_{5/2},p_{3/2},p_{1/2},g_{9/2}$ for the protons and $p_{1/2},g_{9/2},d_{5/2}$ for the neutrons relative to a ^{66}Ni core. In this calculation, which in the following will be referred to as SM1, the 12_2^+ (6275 keV) is a mixed state [42% $\pi(g_{9/2})^4$, 30% πph], while the 12_3^+ (6358 keV) level is a pure πph state. All states at positive parity above the 14_1^+ level are assigned a neutron $g_{9/2}\rightarrow d_{5/2}$ excitation coupled to the $g_{9/2}$ valence protons (νph). At negative parity, the 14_1^- (7970 keV), 15_1^- (8133 keV), and 15_2^- (8501 keV) states are dominated by both proton and neutron excitations ($\pi\nu ph$), whereas all other levels above 14_1^- are νph states. No wave functions are given for the $13_1^+,13_2^-$, and 13_3^- states (compare Table IV of Ref. [4]). Unfortunately, neither excitation energies nor transition probabilities were quoted from this calculation, and thus a systematic comparison to our results is not possible.

B. Shell model calculation by Johnstone and Skouras

Recently, Johnstone and Skouras [5] performed shell model calculations using an ^{88}Sr core and allowing single-particle excitations from the $p_{1/2}$ and $g_{9/2}$ orbits into the $d_{5/2},s_{1/2},d_{3/2},g_{7/2}$ orbits for both protons and neutrons, neglecting, however, the $f_{5/2}$ and $p_{3/2}$ proton orbits (SM2). The interaction used was determined largely by fits to levels of $N=49$ and $N=50$ nuclei; for details we refer to Ref. [5]. First of all, in this calculation the $s_{1/2}$, $d_{3/2}$, and $g_{7/2}$ orbits do not contribute for spins up to $19^+,20^-$. The only exception is the 17_3^- level which in the calculation has a $g_{7/2}$ neutron particle-hole structure. The lowest high-spin states above the yrast 12^+ and 13^- levels were found to be almost pure νph states, with the neutron in the $d_{5/2}$ shell. The only exception is the 12_2^+ (6275 keV) state which was assigned pure proton character. The calculated excitation energies are compared to the experimental ones in Fig. 6. While the overall agreement between experimental and calculated excitation energies is very good, it has been mentioned already in Ref. [5] that the 13_2^- (6919 keV) and the 14_1^- (7970 keV) states ''do not fit in well with the calculated spectrum (unless their assigned spins are in error), and may well be $p_{3/2}$ or $f_{5/2}$ proton hole states.'' To clarify the structure of these states, electromagnetic transition strengths were calculated from the wave functions. For the $B(M1)$ values the effective single-

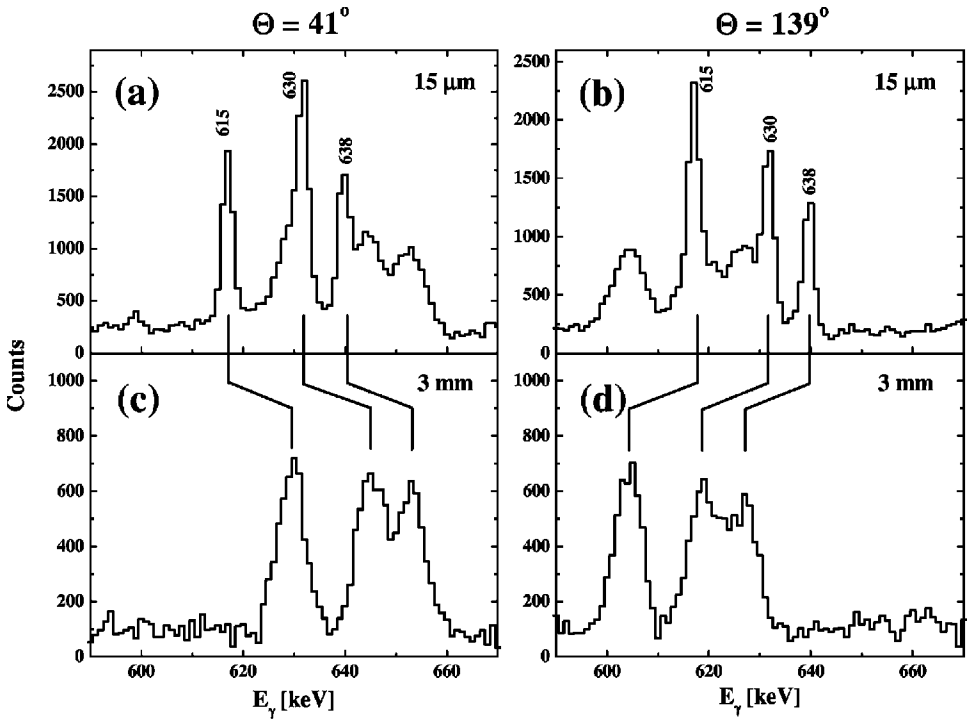

FIG. 5. Part of the coincidence spectra with gates set on both the shifted and the unshifted part of the 725 keV, $12^+ \rightarrow 10^+$ transition in ^{94}Ru. (a) $\Theta = 41°$, 15 μm, (b) $\Theta = 139°$, 15 μm, (c) $\Theta = 41°$, 3 mm, and (d) $\Theta = 139°$, 3 mm.

particle g factors $g_s^{\text{eff}} = 0.7 g_s^{\text{bare}}$ were used, where g_s^{bare} denote the bare-nucleon g factors. As usual, effective charges of $e_\pi = 1.72e$ and $e_\nu = 1.44e$ for protons and neutrons, respectively, were used to calculate $E2$ transition probabilities. First, we assumed the level assignment given in Ref. [5] by lining up the calculated yrast level to the experimental yrast level, the second calculated state of each spin to its second experimental counterpart if observed, and so on. For this assignment, the experimental and calculated transition strengths (dashed lines at negative parity) are compared in Fig. 7. Whereas the agreement at positive parity is very good, it is quite poor at negative parity. Especially the strengths of the $15_2^- \rightarrow 13_3^-$ and $16_1^- \rightarrow 14_3^-$ $E2$ and the $14_3^- \rightarrow 13_1^-, 14_3^- \rightarrow 13_3^-$, and $15_2^- \rightarrow 14_3^-$ $M1$ transitions are underestimated by the shell model calculations by orders of magnitude. As mentioned above there might be a way to remove most of these discrepancies. If we assume that the 13_2^- (6919 keV), 14_1^- (7970 keV), and 15_1^- (8133 keV) levels have significant contributions from configurations other than those considered, the level assignment shown in Fig. 8(b) is obtained. The excellent agreement in excitation energies now applies for all spins as reflected in the decrease of the mean level deviation (MLD) at negative parity from 280 to 100 keV. The MLD at positive parity is 98 keV. As can be seen in Fig. 7, the experimental transition strengths at negative parity are now also well described by the shell model calculations. The most probable configurations of the $13_2^-, 14_1^-$, and 15_1^- states are $p_{3/2}$ or $f_{5/2}$ proton holes coupled to the low-lying $21/2^+$ and $25/2^+$ proton states of ^{95}Rh, which lie at 2.45 and 3.72 MeV. The 13^- state will be a $\pi(f_{5/2})$ hole coupled to the $21/2^+$, the 14^- either a $\pi(p_{3/2})$ or $\pi(f_{5/2})$ hole coupled to the $25/2^+$, and the 15^- a $\pi(f_{5/2})$ hole coupled to the $25/2^+$. The gap between the 13^- and $15^- \pi ph$ states is 1.21 MeV, close to the 1.27 MeV gap between the $21/2^+$ and the $25/2^+$ states in ^{95}Rh.

The degree of mixing of these states, which are outside the present SM2 model space, with neutron particle-hole states (νph) can be deduced from the $M1$ transition strengths observed. The $8501 \rightarrow 8133$ keV transition is between the lowest $\nu ph\, 15^-$ and the $\pi ph\, 15^-$ states. The calculated diagonal $M1$ reduced matrix elements for these two states are 27.9 and $5.9 \mu_N$, and to reproduce the experimental $B(M1) = 0.074\ \mu_N^2$ the mixing of the two states must be only 0.5%. This requires an off-diagonal energy matrix element of 25 keV, and gives a shift of 1.7 keV to the νph state.

The $8272 \rightarrow 7970$ keV transition is between the second $\nu ph 14^-$ and the $\pi ph 14^-$ states. The calculated diagonal $M1$ reduced matrix element for the νph state is 24.3 μ_N, while for the πph state it is 9.8 μ_N for a $p_{3/2}$ hole and 4.4 μ_N for a $f_{5/2}$ hole. To reproduce the experimental $B(M1)$ of 0.194 μ_N^2 then requires mixing of 2.8% for $p_{3/2}$, or 1.4% for $f_{5/2}$. The corresponding off-diagonal energy matrix elements are 48 and 36 keV, respectively, and the shifts to the νph state are 8 and 4 keV. The wave functions of the $\pi ph\, 14^-$ and the lowest $\nu ph\, 15^-$ states determined above can be used to calculate the $8501 \rightarrow 7970$ keV transition strength. The 15^- state is $|15\rangle = 0.998|15(1)\rangle \pm 0.069|15(p)\rangle$ where p refers to proton hole. The intruder 14^- state is $|14\rangle = 0.986|14(p)\rangle \pm 0.166|14(2)\rangle$ for a $p_{3/2}$ hole, or $|14\rangle = 0.993|14(p)\rangle \pm 0.120|14(2)\rangle$ for an $f_{5/2}$ hole. The $M1$ reduced matrix element connecting the 14(2) and 15(1) states is 6.06 μ_N, and between the $f_{5/2}\, 14(p)$ and the $15(p)$ states it is 2.1 μ_N. The $8501 \rightarrow 7970$ keV transition

TABLE II. Experimental reduced electromagnetic transition probabilities in ^{94}Ru deduced in the present work in comparison with the results of the shell model calculation SM2 (see text). The values have been corrected for internal conversion and $\delta=0$ is assumed for all $\Delta I=0,1$ $M1$ transitions.

E_x (keV)	I_i^π	E_γ (keV)	b(%)	I_f^π	σL	$B(\sigma L)^{\rm exp}$ $(e^2\,{\rm fm}^4)/(10^{-3}\,\mu_N^2)$	$B(\sigma L)^{\rm SM}$ $(e^2\,{\rm fm}^4)/(10^{-3}\,\mu_N^2)$
			Positive parity				
3991	10^+	1347	100(3)	8^+	$E2$	>36	216
4716	12^+	725	98(3)	10^+	$E2$	116(6)	115
6614	13^+	1898	80(2)	12^+	$M1$	5.3(7)	0.8
		257[a]	20(2)	12_3^+	$M1$	520(90)	129
7157	14^+	543	97(2)	13^+	$M1$	720(90)	1125
		2441	3(1)	12^+	$E2$	0.6(2)	0.2
7773	15^+	615[a]	77(5)	14^+	$M1$	>470	230
		1159	23(2)	13^+	$E2$	>224	128
8411	16^+	638	68(3)	15^+	$M1$	>140	606
		501[a]	20(4)	15_2^+	$M1$	>70	771
		1254	12(1)	14^+	$E2$	>29	202
9041	17^+	630	89(2)	16^+	$M1$	>100	532
		1268	11(1)	15^+	$E2$	>12	236
9526	18^+	485[a]	82(9)	17^+	$M1$	780(100)	642
		1116[a]	18(6)	16^+	$E2$	163(55)	125
9920	19^+	394	76(4)	18^+	$M1$	>134	120
		879	24(3)	17^+	$E2$	>65	123
			Negative parity				
2624	5^-	438	68(2)	4^+	$E1$		
		127	32(1)	6^+	$E1$		
4489	11^-	292	32(1)	9^-	$E2$	109(6)	226
		498	67(1)	10^+	$E1$		
		151	1(1)	9_2^-	$E2$	73(73)	55
5568	13^-	1079	100(3)	11^-	$E2$	192(22)	177
8272	14_3^-	2704	77(5)	13^-	$M1$	5.3(6)	0.4
		503[a]	12(5)	13_3^-	$M1$	127(54)	747
		302	4(1)	14^-	$M1$	194(52)	-
		120	7(1)	14_2^-	$M1$	4600(800)	2.4
8501	15_2^-	230	44(1)	14_3^-	$M1$	1080(80)	1185
		349	17(1)	14_2^-	$M1$	122(11)	40
		368	12(1)	15^-	$M1$	74(8)	-
		532	14(1)	14^-	$M1$	29(3)	-
		733	12(1)	13_3^-	$E2$	251(27)	207
8996	16^-	495	83(2)	15_2^-	$M1$	>385	677
		260	9(1)	15_3^-	$M1$	>250	1139
		725[a]	8(2)	14_3^-	$E2$	>244	204
9928	18^-	932	30(1)	16^-	$E2$	69(5)	138
		140	37(1)	17_2^-	$M1$	1360(100)	2963
		674	23(1)	17^-	$M1$	8(1)	0.3
		793[a]	11(2)	16_2^-	$E2$	57(11)	100
11042	20^-	1113	81(3)	18^-	$E2$	>140	183
		597	19(1)	19^-	$M1$	>18	9

[a]Part of unresolved dublet in [3]; the intensity is estimated.

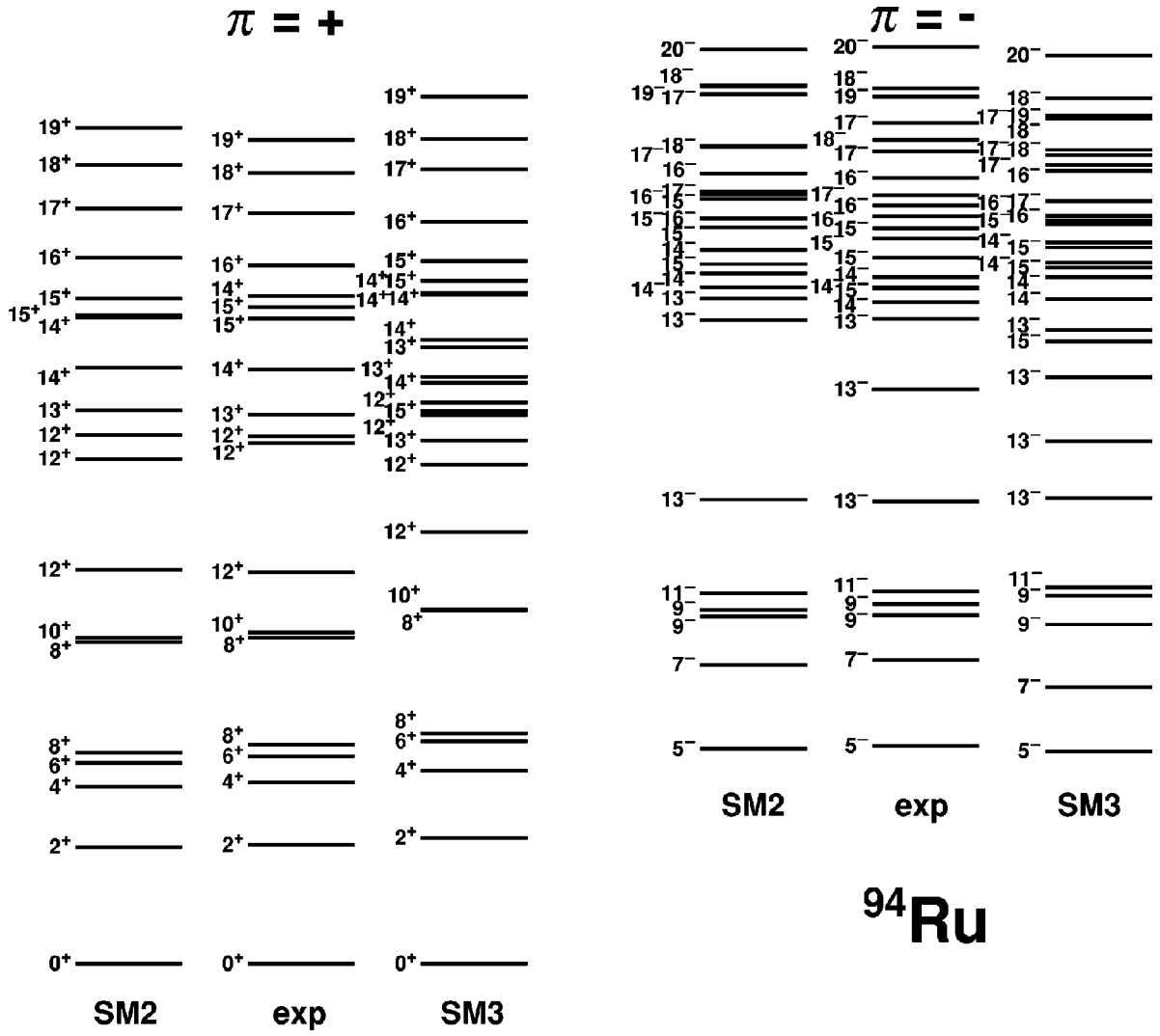

FIG. 6. Excitation energies in ^{94}Ru obtained in the shell model calculations SM2 and SM3 in comparison with the experimental values for the positive parity on the left and the negative parity on the right.

probability is therefore 0.032 μ_N^2 for a $p_{3/2}$ hole, and either 0.024 or 0.011 μ_N^2 (depending on phases) for an $f_{5/2}$ hole. The experimental value is 0.029(3) μ_N^2, so either hole (or a mixture) is possible.

The only remaining serious discrepancy concerns the 8272→8152 keV transition connecting the second and the first $\nu ph\,14^-$ states (compare Fig. 7). SM2 gives a weak $M1$ decay, while experiment suggests that it is extremely large. For the determination of the experimental value, we rely on the placement of the 120 keV γ ray and its intensity quoted in Ref. [3].

C. Calculations in an extended proton space

We performed shell model calculations considering a model space consisting of $f_{5/2}, p_{3/2}, p_{1/2}, g_{9/2}$ proton and $g_{9/2}, d_{5/2}$ neutron orbitals relative to a ^{68}Ni core. The justification for not including any further neutron orbits above the $N=50$ gap, e.g., the $g_{7/2}$ orbit, which in ^{95}Rh is as close in energy as 0.94 MeV [13] to the $d_{5/2}$ orbit, was the observation of high-energy γ rays ($E_\gamma > 2$ MeV) above $19^+, 20^-$ in ^{94}Ru and $39/2^+, 39/2^-$ in ^{95}Rh. This gap above the maximum spins of the $\pi(g_{9/2})^{4,5} \otimes [\nu(g_{9/2})^{-1}\ \nu(d_{5/2})]$ and $[\pi(g_{9/2})^{5,6}\pi(p_{1/2})^{-1}] \otimes [\nu(g_{9/2})^{-1}\nu(d_{5/2})]$ configurations in both nuclei indicates that $d_{5/2}$ is the only relevant orbit. The effective interactions in the proton shells were taken from the work of Ji and Wildenthal [14]. For the proton-neutron interaction connecting the $\pi(p_{1/2}, g_{9/2})$ and the $\nu g_{9/2}$ orbitals, the two-body matrix elements (TBME) given by Gross and Frenkel [15] were used. Empirical TBME were taken for the $\nu(g_{9/2}) \otimes \nu(d_{5/2})$ [16] and $\pi(f_{5/2}) \otimes \nu(g_{9/2})$ [17] multiplets, while the surface delta interaction (SDI) was used for the remaining TBME [18]. The single-particle energies of the proton orbitals relative to the ^{68}Ni core were taken to reproduce those relative to ^{78}Ni [14]. Similarly, the neutron single-particle energies were adopted to fit the neutron single-hole energy of the $g_{9/2}$ orbital [15] and the neutron single-particle energy of the $d_{5/2}$ shell [19], relative to a ^{88}Sr core. More detailed information about all parameters used can be found in the paper by Winter *et al.* [18]. The only restriction we applied in our calculations, which were per-

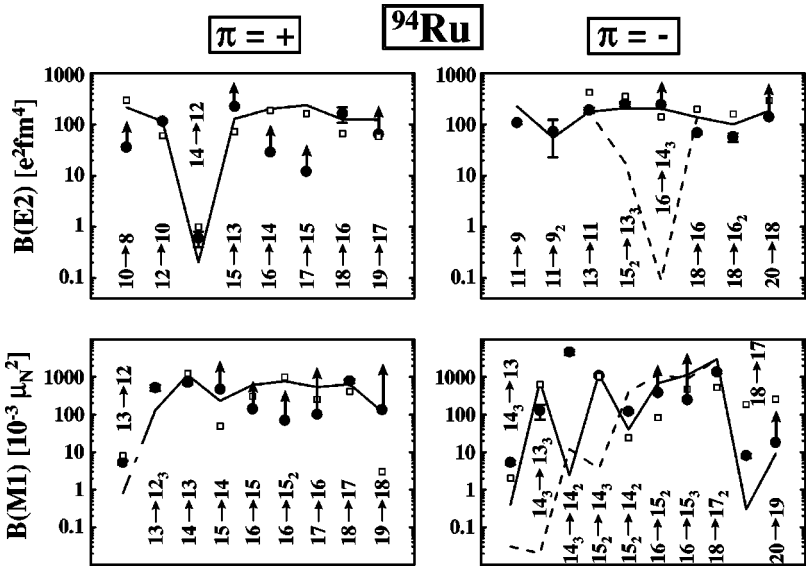

FIG. 7. Comparison between experimental and theoretical (SM2, SM3) transition strengths for $M1$ and $E2$ transitions in ^{94}Ru. The results for the positive parity are shown on the left, the results for the negative parity on the right. The experimental values are marked by filled circles with error bars and labelled by the initial and final spins. The SM2 values resulting from the assignment shown in Fig. 8 are given as full lines, whereas the dashed line at negative parity marks the calculated values assuming the assignment in Ref. [5]. The results from the SM3 calculation with the assignments from Fig. 8 are given as open squares.

formed using the computer code RITSSCHIL [20], is that the excitation of only one neutron from the $g_{9/2}$ orbital over the shell gap into the $d_{5/2}$ orbital was allowed. In the following, this calculation will be referred to as SM3. Note that all parameters are identical to the ones recently used not only to describe the excitation energies, but furthermore to successfully reproduce the electromagnetic transition strengths in ^{95}Rh [1]. As can be seen in Fig. 6, where the excitation energies obtained in this calculation are compared to the experimental values, the level sequences in ^{94}Ru are not as well reproduced by SM3 as it has been the case in ^{95}Rh [1]. Especially for the spins, which can be either built by pure proton configurations containing $f_{5/2}$ excitations or neutron core-excited configurations (13^+–15^+,14^-,15^-), a definite assignment between calculated and experimental states solely on the basis of excitation energies is not possible.

However, we have already additional information from the discussion in the last section. There, we saw that all states at positive parity can be well understood without considering proton excitations. In SM3, the calculated 12_2^+,13_1^+,12_3^+,15_1^+, and 14_1^+ states are all of the πph type and therefore seem to have no experimental equivalent. Instead, the levels were assigned as shown in Fig. 8(a). At negative parity, we came to the conclusion that the experimental 13_2^-,14_1^-, and 15_1^- states are proton particle-hole states. We assigned these levels to the calculated πph states $[\pi(f_{5/2})^{-1}\ \pi(g_{9/2})^{3,5}]$ as shown in Fig. 8(b). The calculated 13_2^- level is a mixed state [34% $\pi(p_{1/2})^{-1}\pi(g_{9/2})^5$, 51% $\pi(f_{5/2})^{-1}\pi(g_{9/2})^3$] and is not observed experimentally. The MLD for the SM3 calculation with the assignments from Fig. 8 is 399 and 234 keV for the positive and negative parity states, respectively. It should be mentioned that most of the neutron core-excited states at negative parity have additional significant (typically 30–50%) contributions from proton excitations. At positive parity, this is only the case for the 19_1^+ level. In Fig. 7, the transition strengths obtained from the SM3 wave functions are compared to the experimental values.

D. Analogies between ^{94}Ru and ^{95}Rh

Finally, we will compare the transition strengths obtained at positive parity in ^{94}Ru in the present work to the strengths at negative parity in ^{95}Rh [1]. On the proton side, the $\pi=+$ states in ^{94}Ru are built from four unpaired protons in the $g_{9/2}$ orbit. On the other hand, the negative parity levels in ^{95}Rh consist of five active protons, that is four proton holes in the $g_{9/2}$ plus one proton or proton hole in the $p_{1/2}$ orbit. If the $p_{1/2}$ proton acts only as a spectator, one would expect that corresponding states differing by $1/2\hbar$ in spin should have the same structure and the transitions between these states therefore comparable strengths. Note, that $p_{1/2}$ does not contribute to the $E2$ matrix element, and that the $M1$ transitions are dominated by the large $\pi(g_{9/2})$ magnetic moment. In Fig. 9, the transition probabilities for the transitions $I_i^+ \rightarrow I_f^+$ in ^{94}Ru and $(I_i+1/2)^- \rightarrow (I_f+1/2)^-$ in ^{95}Rh are shown for all those cases where the corresponding strengths were determined in both nuclei. The similarity is apparent: strong $E2$ transitions with $B(E2) \approx 100\ e^2\mathrm{fm}^4$ were observed for the $19^+ \rightarrow 17^+$,$18^+ \rightarrow 16^+ \rightarrow 14^+$,$12^+ \rightarrow 10^+ \rightarrow 8^+$ and $39/2^- \rightarrow 35/2^-$, $37/2^- \rightarrow 33/2^- \rightarrow 29/2^-$, $25/2^- \rightarrow 21/2^- \rightarrow 17/2^-$ transitions, respectively, mainly due to allowed recouplings of the $\pi(g_{9/2})^n$ parts of the wave functions with $\Delta I_\pi = 2$. Only the $14^+ \rightarrow 12^+$ and $29/2^- \rightarrow 25/2^-$ transitions from the decay of the neutron core-excited states are dramatically retarded. The experimental values $B(E2;\ 14^+ \rightarrow 12^+) = 0.6(2)\ e^2\mathrm{fm}^4$ and $B(E2;\ 29/2^- \rightarrow 25/2^-) = 3.1(3)\ e^2\mathrm{fm}^4$ are by about two orders of magnitude lower than those for

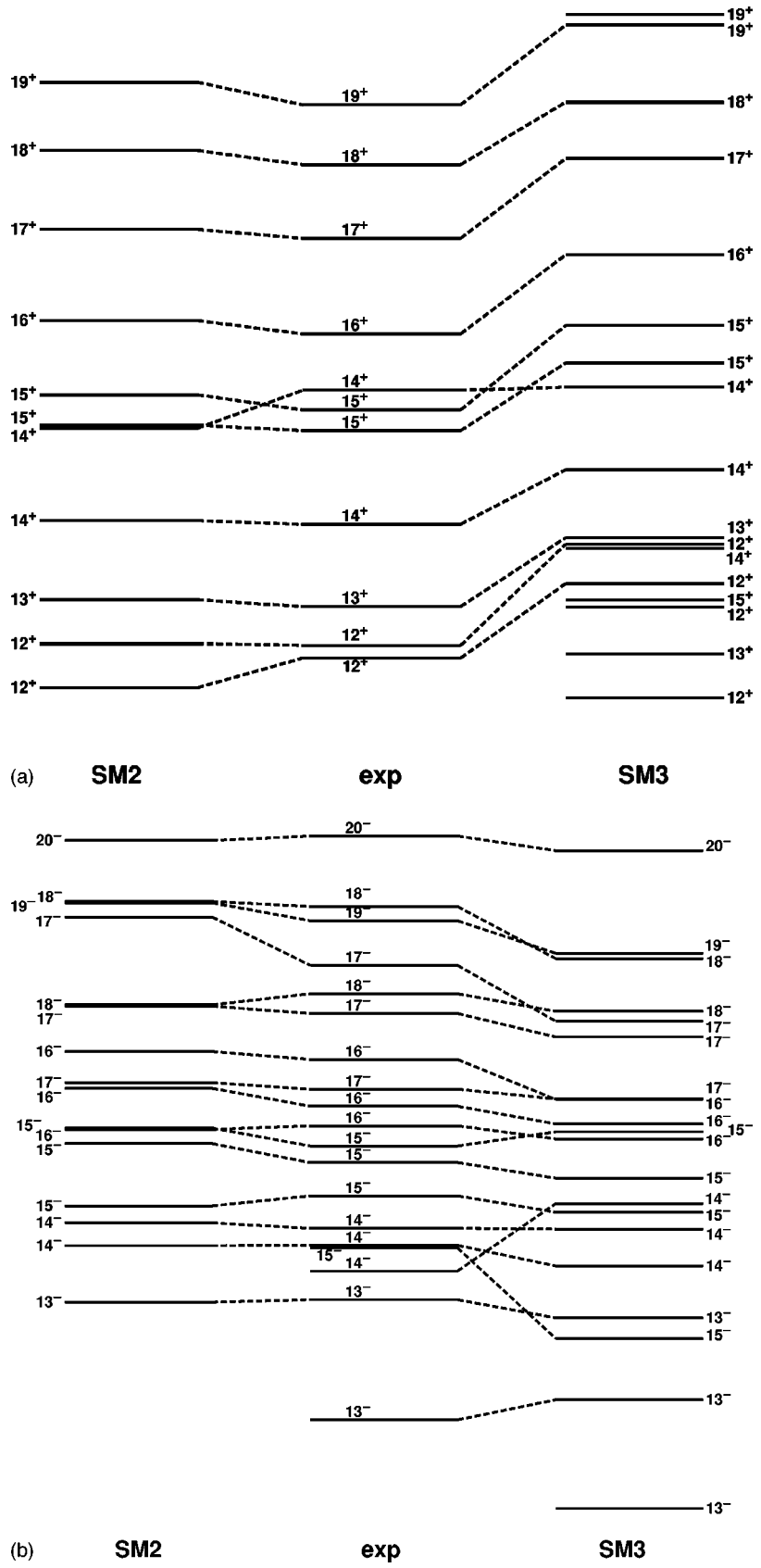

FIG. 8. Comparison between experimental and calculated (SM2, SM3) excitation energies in ^{94}Ru for (a) the positive parity and (b) the negative parity.

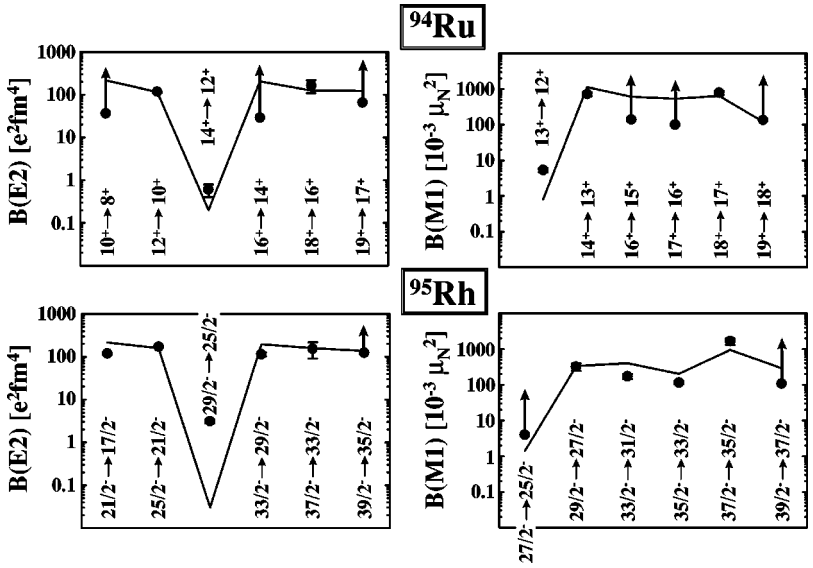

FIG. 9. Comparison between transition strengths at positive parity in ^{94}Ru and at negative parity in ^{95}Rh. The experimental values are marked by filled circles with error bars and labeled by the initial and final spins. The shell model values (SM2) are given as full lines.

the allowed $E2$ transitions. In both nuclei, sequences of rather strong $M1$ transitions in the range 0.1–1 μ_N^2 were observed which come about by recoupling only the two unpaired neutrons $[\nu(g_{9/2})^{-1}\,\nu(d_{5/2})]$ to different spins while keeping the proton parts of the wavefunctions constant. The $13^+ \rightarrow 12^+$ and $27/2^- \rightarrow 25/2^-$ transitions, on the other hand, require a $d_{5/2} \rightarrow g_{9/2}$ neutron transition and are not allowed. For symmetry reasons, a similarity is also expected between the $\pi = -$ states in ^{94}Ru and the $\pi = +$ levels in ^{95}Rh. However, in this case the experimental information available unfortunately does not allow for such a systematic comparison as discussed above.

V. CONCLUSIONS

Accurate lifetimes in ^{94}Ru obtained from a high-statistics $\gamma\gamma$ coincidence RDDS experiment via the reaction ^{58}Ni(^{40}Ca, $4p$) have been presented. The experimental high-spin states and electromagnetic decay properties of ^{94}Ru were compared to shell model calculations based on an extended configuration space, including one-particle-one-hole excitations across the $N=50$ neutron shell. The 13_2^- (6919 keV), 14_1^- (7970 keV), and 15_1^- (8133 keV) states have been identified by means of the decay strengths to be intruder states involving either $p_{3/2}$ or $f_{5/2}$ proton holes, but no neutron excitation. All other levels above 6.3 MeV contain one neutron being excited from the $g_{9/2}$ into the $d_{5/2}$ orbit. The similarity between the strengths of transitions at positive parity in ^{94}Ru and at negative parity in ^{95}Rh indicates that the $(I+1/2)^-$ levels in ^{95}Rh can be regarded as a $p_{1/2}$ proton coupled to the I^+ state in ^{94}Ru, in the sense of a simple weak-coupling picture.

ACKNOWLEDGMENTS

We are most grateful to Dr. Repnow and the crew of the Heidelberg tandem accelerator for their friendly and efficient cooperation. The EUROBALL project is funded by Deutsches Bundesministerium für Bildung, Wissenschaft, Forschung und Technologie (BMBF).

[1] A. Jungclaus, D. Kast, K.P. Lieb, C. Teich, M. Weiszflog, T. Härtlein, C. Ender, F. Köck, D. Schwalm, J. Reif, R. Peusquens, A. Dewald, J. Eberth, H.-G. Thomas, M. Górska, and H. Grawe, Nucl. Phys. **A637**, 346 (1998).

[2] E. Nolte, G. Korschinek, and U. Heim, Z. Phys. A **298**, 191 (1980).

[3] H.A. Roth, S.E. Arnell, D. Foltescu, Ö. Skeppstedt, J. Blomqvist, A. Nilsson, T. Kuroyanagi, S. Mitarai, and J. Nyberg, Phys. Rev. C **50**, 1330 (1994).

[4] S.S. Ghugre and S.K. Datta, Phys. Rev. C **52**, 1881 (1995).

[5] I.P. Johnstone and L.D. Skouras, Phys. Rev. C **55**, 1227 (1997).

[6] A. Dewald, P. Sala, R. Wrzal, G. Böhm, D. Lieberz, G. Siems, R. Wirowski, K.O. Zell, A. Gelberg, P. von Brentano, P. Nolan, A.J. Kirwan, J. Bishop, R. Julin, A. Lampinen, and H. Hattula, Nucl. Phys. **A545**, 822 (1992).

[7] C. Lingk, A. Jungclaus, D. Kast, K.P. Lieb, C. Teich, M. Weiszflog, C. Ender, T. Härtlein, F. Köck, D. Schwalm, A. Dewald, J. Eberth, R. Peusquens, H.G. Thomas, M. Górska, and H. Grawe, Phys. Rev. C **56**, R2349 (1997).

[8] J. Eberth, H.G. Thomas, P. von Brentano, R.M. Lieder, H.M. Jäger, H. Kämmerling, M. Berst, D. Gutknecht, and R. Henck, Nucl. Instrum. Methods Phys. Res. A **369**, 135 (1996).

[9] T. Härtlein and O. Koschorreck, Jahresbericht, 1995, Max-Planck-Institut für Kernphysik, Heidelberg (unpublished).

[10] C.M. Lederer, J.M. Jaklevic, and J.M. Hollander, Nucl. Phys. **A169**, 449 (1971).
[11] H. Grawe, H.H. Bertschat, and H. Haas, Hyperfine Interact. **15/16**, 65 (1983).
[12] G. Böhm, A. Dewald, P. Petkov, and P. von Brentano, Nucl. Instrum. Methods Phys. Res. A **329**, 248 (1993); A. Dewald, S. Harissopulos, and P. von Brentano, Z. Phys. A **334**, 163 (1989).
[13] *Table of Isotopes*, 8th ed., edited by R. B. Firestone *et al.* (Wiley, New York, 1996).
[14] X. Ji and B.H. Wildenthal, Phys. Rev. C **37**, 1256 (1988).
[15] R. Gross and A. Frenkel, Nucl. Phys. **A267**, 85 (1976).
[16] P.C. Li and W.W. Daehnick, Nucl. Phys. **A462**, 26 (1987).
[17] P.C. Li, W.W. Daehnick, S.K. Saha, J.D. Brown, and R.T. Kouzes, Nucl. Phys. **A469**, 393 (1987).
[18] G. Winter, R. Schwengner, J. Reif, H. Prade, L. Funke, R. Wirowski, N. Nicolay, A. Dewald, P. von Brentano, H. Grawe, and R. Schubart, Phys. Rev. C **48**, 1010 (1993).
[19] K. Muto, T. Shimano, and H. Horie, Phys. Lett. **135B**, 349 (1984).
[20] D. Zwarts, Comput. Phys. Commun. **38**, 365 (1985).